Decay rates of internal waves in a fluid near the liquid-vapor critical point

K. F. Gurski
USRA, Center of Excellence in Space Data and Information Sciences, NASA Goddard Space Flight Center, 930.5, Greenbelt, Maryland 20771

R. L. Pego
Department of Mathematics and Institute for Physical Science and Technology, University of Maryland, College Park, Maryland 20742

(Received 30 November 1999)

We study the damping of internal waves in a viscous fluid near the liquid-vapor critical point. Such a fluid becomes strongly stratified by gravity due to its large compressibility. Using the variable-density incompressible Navier-Stokes equations, we model an infinite fluid layer with rigid horizontal boundaries and periodic side boundary conditions. We present operator-theoretic results that predict the existence of internal-wave modes with arbitrarily small damping rates. We also solve the eigenvalue problem numerically using a compound matrix shooting method and a second method based on a matched-asymptotic perturbation expansion for small viscosity. At temperatures far above the critical point, the damping of the internal waves is substantially influenced by both boundary layer and volumetric effects. The boundary layer effect is caused by horizontal shearing layers near the two fixed horizontal boundaries. As the temperature approaches the critical temperature, an additional internal shearing layer develops as the density stratification curve steepens on approach to the two-phase regime. Numerical calculations show that for some of the internal-wave modes this causes a dramatic increase in the damping rate that dominates the boundary layer effects.

PACS number(s): 47.55.Hd, 68.35.Rh, 02.60.Lj, 47.11.+j

I. INTRODUCTION

Close to the liquid-vapor critical point, the physical characteristics of a fluid change rapidly. For example, the compressibility diverges to infinity. By consequence, density becomes strongly stratified by gravity, even in the one-phase regime. Thus near-critical fluids are able to support internal gravity waves.

Internal waves are common to a variety of large-scale physical phenomena, including the fluid motion in a lake, ocean, planetary atmosphere, or stellar interior [1,2]. Because of the singularities that occur at the critical point, however, internal waves in near-critical fluids can be observed in the laboratory in very small volumes of fluid. In recent experiments at the National Institute for Standards and Technology (NIST), Berg *et al.* [3] studied internal gravity waves in near-critical xenon contained in a small cell with immersed apparatus configured as a viscometer. Using an inviscid incompressible fluid model, they calculated the frequencies of the internal-wave motion and compared these with their experimental results. Later, Anderson and McFadden [4] introduced a diffuse interface model of the near-critical fluid to study the two-phase regime. Boukari [5] has also observed internal waves in near-critical xenon in a cell designed for fluctuation measurements on the space shuttle [6,7].

These experimentalists report observing damping of internal waves that is not explained by fluid models used to date. Here we aim to study wave damping by including the viscous effects neglected in [3,4] and looking for normal modes in a layer of stably stratified fluid with rigid boundaries above and below.

In such a damped system, one hopes to identify the slowest decaying modes with a given horizontal wave number since these should dominate the long-time behavior. Surprisingly, here we find that there exists an infinite number of nonoscillatory internal-wave modes with arbitrarily small damping rates. A similar result has long been known for surface waves in a constant-density fluid neglecting surface tension [8]; however, surface tension tends to strongly damp these modes [see [9], Eq. (18)]. For an analytical treatment of the case of an exponential density profile (corresponding to an ideal fluid) with constant kinematic viscosity and the Boussinesq approximation in a two-dimensional closed container, see [10].

We also numerically compute decay rates of oscillatory modes for near-critical xenon with parameters roughly corresponding to the cell geometry in the experiments of Berg *et al.* At temperatures well above critical, a substantial fraction of wave damping is due to a boundary layer effect, caused by viscous dissipation in horizontal shearing layers near the two fixed boundaries. As the temperature approaches critical, an additional horizontal shearing layer develops at the center of the fluid layer as the density stratification profile steepens on approach to the two-phase regime. For some of the internal-wave modes this causes a dramatic increase in the damping rate that dominates the boundary layer effects.

II. THE MODEL EQUATION

We begin the analysis by modeling an infinite layer of fluid, confined between rigid horizontal boundaries at $z = \pm L$, using the variable-density incompressible Navier-Stokes equations. Viscosity is modeled in two ways, first by taking the shear viscosity μ as a constant, and second by using the viscosity model of [11] at zero frequency with correlation length given by the restricted cubic model [12].

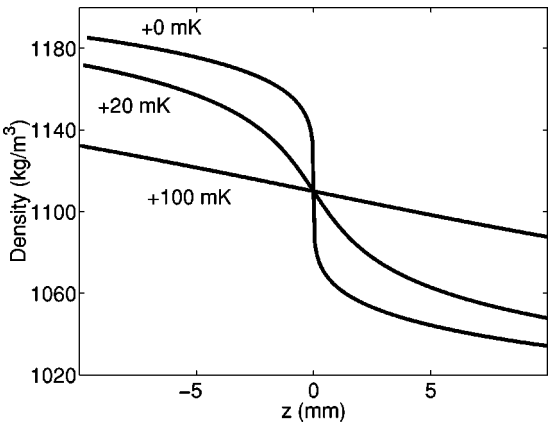

FIG. 1. Density stratification of near-critical xenon as a function of depth in a cell of length 19 mm using the restricted cubic density profile calculated at various temperatures above the critical temperature.

We impose periodic boundary conditions in the horizontal directions.

At first, the idea of modeling a near-critical fluid as incompressible seems like a paradox, since it is exactly the high compressibility of the fluid near the critical point that is responsible for density stratification. However, a satisfactory justification of the use of the incompressibility assumption for this problem can be given by an asymptotic expansion for low-speed, near-critical flow as performed by Denny and Pego [13]. By choosing to keep the combination of pressure and density as thermodynamic variables rather than the combination of density and temperature in the low-Mach-number approximation, one can arrive at the variable-density Navier-Stokes model [14]. This consists of the standard incompressible Navier-Stokes equations with gravity, and a nonconstant density that is convected with the flow.

In equilibrium, the density profile $\rho(z)$ is continuously vertically stratified at temperatures above the critical temperature T_c. A graph of the density stratification in near-critical xenon in Earth's gravity is shown in Fig. 1. We use the restricted cubic [15,12] and van der Waals equations of state (as in [4]) to model the density stratification found near the critical point. We linearize the equations around an equilibrium state and look for normal modes. Thus, the vertical velocity is required to have the form $W(x,y,z,t) = e^{i(k_x x + k_y y) - \lambda t} w(z)$ where $-i\lambda$ represents the complex frequency. The horizontal velocities, pressure, and density perturbations have similar expressions, but may be eliminated to generate a single fourth-order ordinary differential equation for the vertical velocity profile $w(z)$.

For near-critical xenon the shear viscosity $\mu(\xi)$ diverges as the liquid-vapor critical point is approached as $\xi^{0.069}$, where ξ is the correlation length. Because this divergence is weak, modeling viscosity as a constant is a reasonable first approximation. In this case of constant viscosity one obtains

$$\frac{\mu}{\rho(z)}(D^2-k^2)^2 w(z) + \lambda(D^2+\alpha(z)D-k^2)w(z) + \frac{\alpha(z) g k^2}{\lambda} w(z) = 0, \tag{1}$$

with four boundary conditions, $w(-L)=w(L)=Dw(-L)=Dw(L)=0$, where $D=\partial/\partial z$, $\alpha(z)=D\rho(z)/\rho(z)$, and $k^2 = k_x^2 + k_y^2$. We assume $k \neq 0$. This is a nonlinear eigenvalue problem; one should find λ so that Eq. (1) has a nontrivial solution satisfying the four boundary conditions indicated.

From the solution of this problem one determines that the full velocity $\mathbf{u}=(U,V,W)$ and density perturbation $\delta\rho$ have the following normal mode form:

$$\mathbf{u} = e^{ik_x x + ik_y y - \lambda t}\left(\frac{ik_x}{k^2} Dw(z), \frac{ik_y}{k^2} Dw(z), w(z)\right), \tag{2}$$

$$\delta\rho = e^{ik_x x + ik_y y - \lambda t} \frac{w(z) D\rho(z)}{\lambda}. \tag{3}$$

If we replace the assumption of constant shear viscosity with the more physical viscosity model of [11] at zero frequency we have the viscosity as a function of correlation length. For a fixed temperature, the correlation length is a function of the density, which in turn is a function of height. Therefore if we use the restricted cubic model for correlation length [12], then the viscosity in equilibrium is a function of height. Instead of Eq. (1) we have the nonlinear eigenvalue problem

$$\frac{D^2\mu(z)}{\rho(z)}(D^2+k^2)w(z) + \frac{2D\mu(z)}{\rho(z)}(D^2-k^2)Dw(z) + \frac{\mu(z)}{\rho(z)}(D^2-k^2)^2 w(z) + \lambda(D^2+\alpha(z)D-k^2)w(z) + \frac{\alpha(z) g k^2}{\lambda} w(z) = 0, \tag{4}$$

with four boundary conditions, $w(-L)=w(L)=Dw(-L)=Dw(L)=0$.

III. NONOSCILLATORY MODES

We have employed operator-theoretic methods to establish some fundamental properties of the damping rates determined by Eq. (1) for a general stably stratified density profile $\rho(z)$, one that satisfies $D\rho(z)<0$. By adapting the abstract approach used in the analysis of the damping of free-surface water waves by Askerov *et al.* [8] and using the Keldysh completeness theorem (see [16]), we prove [17]

Theorem 1. The eigenvalues of Eq. (1) form a countably infinite set contained in the half plane $Re\lambda > 0$. At most a finite number are nonreal. There exist both an infinite number of real eigenvalues converging to zero and an infinite number converging to infinity, and there is no other accumulation point.

This result indicates that there are nonoscillatory wave modes with arbitrarily small damping rates in any periodically confined stably stratified viscous fluid layer. This is surprising since naively one expects a purely discrete spectrum like that of a parabolic equation in a bounded domain. Instead it turns out that $\lambda = 0$ is an accumulation point for eigenvalues. Thus one cannot expect a uniform exponential rate of decay to equilibrium in the dynamic problem. A similar theorem is proved in [10] for the exponentially stratified

case with the Boussinesq approximation in an arbitrary two-dimensional domain.

For a physical explanation for this behavior, suppose that the kinematic viscosity $\nu=\mu/\rho$ is constant and $\alpha<0$ is constant, which corresponds to the case of an exponentially stratified fluid. Then Eq. (4) has constant coefficients and may be written

$$\lambda^2(D^2+\alpha D-k^2)w+\alpha g k^2 w+\lambda\nu(\alpha^2(D^2+k^2) +2\alpha(D^3-k^2D)+(D^2-k^2)^2)w =0. \tag{5}$$

We ignore the boundary conditions and reintroduce general time dependence, writing $w(z,t)=\hat{w}(t)e^{inz}$ and consider n large. The resulting equation,

$$(n^2\partial_t^2-\alpha g k^2)\hat{w}(t)+\nu n^4\partial_t\hat{w}(t)\approx 0, \tag{6}$$

corresponds to an overdamped oscillator with decay rates given by

$$\lambda=\frac{\nu n^2}{2}\pm\sqrt{\frac{\nu^2 n^4}{4}+\frac{\alpha g k^2}{n^2}}\approx\begin{cases}\nu n^2 & \text{for } +\\ \dfrac{-\alpha g k^2}{\nu n^4} & \text{for } -.\end{cases}$$

For n large, the $+$ case gives the fast decay one expects from parabolic dissipation, but the $-$ case gives very slow decay. In the absence of viscosity these modes correspond to slow oscillations of the thin fluid layers between consecutive points where vertical velocity vanishes. The introduction of viscosity highly overdamps these waves and separates them into fast- and slow-decaying nonoscillatory modes.

For a more precise description, we can take account of the boundary conditions, using the method of matched-asymptotic expansions [18] to determine an expression for the arbitrarily small eigenvalues. We begin with Eq. (5) and with the boundary conditions that $w=Dw=0$ at $z=\pm L$. In this perturbation problem we have two inner boundary layers at $z=\pm L$ where we introduce stretched variables $\zeta_\pm=(L\pm z)/\lambda^{1/4}$, and in the outer region we use the scaled variable $\xi=z/\lambda^{1/4}$. Carrying out the expansion and matching procedure we find

$$\lambda\approx-\alpha g k^2\nu^{-1}\left(\frac{(2n+1)\pi}{4L}\right)^{-4}, \tag{7}$$

where n is an integer corresponding to the vertical wave number. As n approaches infinity, the eigenvalues approach zero with the same n^{-4} dependence as found above for slow-decaying modes when the boundary conditions are ignored.

Arbitrarily small damping rates in the presence of viscosity were predicted for water waves with a free surface and no surface tension [8]. In that case they arise in the limit of large horizontal wave number ($k\to\infty$), which is different from the case of stratified fluids considered here. If one includes the effects of surface tension, however, free-surface damping rates are no longer arbitrarily small, and in fact the results of Martel and Knobloch [[9], Eq. (18)] indicate that high-frequency waves are always damped quite strongly unless the water is very deep (on the order of hundreds of meters). By contrast, the damping of internal waves in stratified fluids is not subject to the effects of surface tension, and modes with arbitrarily slow damping rates should be of physical significance.

IV. OSCILLATORY MODES

In this section we concentrate on computing the decay rates for the damped oscillatory internal-wave modes. By variational methods we can prove the following theoretical bounds concerning the location of the eigenvalues for oscillatory modes in the complex plane [17].

Theorem 2. All nonreal eigenvalues of Eq. (1) *are in the half ring where* $Re\lambda>0$ *and*

$$\frac{\mu(\pi^2/4L^2+k^2)}{2\max_z\rho(z)}\leqslant|\lambda|\leqslant\frac{2g\max_z|\rho'(z)|}{\mu k^2}. \tag{8}$$

There are therefore no oscillatory modes if the viscosity is large enough, satisfying

$$\mu\geqslant\sqrt{\frac{4g\max_z\rho(z)\max_z|\rho'(z)|}{k^2(\pi^2/4L^2+k^2)}}. \tag{9}$$

A. Numerical methods

We employ two different numerical methods to solve the z-velocity equation (1) for the eigenvalues and eigenfunctions.

1. Asymptotic expansion

The first method utilizes matched-asymptotic perturbation expansions for small viscosity with two boundary layers at $z=\pm L$ (in the constant-viscosity case). With small viscosity the fluid is essentially inviscid away from the boundaries, and the effects of the nonzero viscosity will be felt only in a small region near each boundary. For the inner expansion in the boundary layer near $z=-L$ we apply the stretching transformation $\xi=(z+L)/\sqrt{\mu}$ and near $z=L$ we use $\eta=(L-z)/\sqrt{\mu}$. Matching the inner boundary layer expansions to the outer expansion determines in a standard fashion boundary conditions for terms in the outer expansion.

We suppress the details of the matching procedure and describe the results in terms of the outer expansion. We write $w(z)=\psi(z)\sqrt{\rho(-L)/\rho(z)}$ and expand the eigenvalue and eigenfunction as follows:

$$\lambda=\lambda_0+\sqrt{\mu}\lambda_1+\mu\lambda_2+O(\mu^{3/2}), \tag{10}$$

$$\psi=\psi_0+\sqrt{\mu}\psi_1+\mu\psi_2+O(\mu^{3/2}). \tag{11}$$

Then at order $O(1)$ the z-velocity equation (1) reduces to the Sturm-Liouville problem

$$D^2\psi_0(z)+q(z)\psi_0(z)-\tau\alpha(z)\psi_0(z)=0 \tag{12}$$

with the boundary conditions $\psi_0(-L)=\psi_0(L)=0$. Here $\tau=-gk^2/\lambda_0^2$. This problem has an infinite number of solutions, indexed by an integer n taking values 1,2,3, ... It is

solved numerically using a double precision version of the Sturm-Liouville solver SLEIGN [19] to find $\psi_0(z)$ and τ (hence λ_0) for given n.

At order $O(\sqrt{\mu})$ we find that

$$D^2\psi_1(z)+q(z)\psi_1(z)=\tau\alpha(z)\left(\psi_1(z)-\frac{2\lambda_1}{\lambda_0}\psi_0(z)\right),$$
$$\psi_1(-L)=-\frac{1}{\beta}D\psi_0(-L), \quad \text{and} \quad \psi_1(L)=\frac{1}{\delta}D\psi_0(L), \tag{13}$$

where $\beta=-i\sqrt{\lambda_0\rho(-L)}$ and $\delta=-i\sqrt{\lambda_0\rho(L)}$. We multiply Eq. (13) by $\psi_1(z)$ and integrate with respect to z from $-L$ to L. Since SLEIGN provides the information to algebraically calculate $D\psi_0(-L)$ and $D\psi_0(L)$ we can calculate λ_1 from the following equation:

$$\lambda_1=\frac{\sqrt{\rho(L)}[D\psi_0(L)]^2+\sqrt{\rho(-L)}[D\psi_0(-L)]^2}{2i\tau(\sqrt{\lambda_0})^{-1}}. \tag{14}$$

To achieve a smooth ψ_0 we used the two-point boundary value problem solver DBVSUP [20] to recalculate ψ_0 now that we have a value for λ_0. We chose to normalize ψ_0 by $\int_{-L}^{L}\alpha(z)\psi_0^2(z)dz=-1$.

To solve for λ_2 we must numerically calculate ψ_1. We used DBVSUP to calculate ψ_1. Since ψ_1 is nonunique, we can write $\psi_1=\phi-N\psi_0$ where N is an arbitrary complex number. We choose N such that $\int_{-L}^{L}\alpha(z)\psi_0(z)\psi_1(z)dz=0$. We find that λ_2 is given by

$$\lambda_2=\frac{-\lambda_0}{2\tau}D\psi_0\psi_2\Big|_{-L}^{L}+\frac{3\lambda_1^2}{2\lambda_0}+\frac{\alpha}{2\tau\rho(z)}[D\psi_0(z)]^2\Big|_{-L}^{L}$$
$$+\frac{1}{2\tau}\int_{-L}^{L}\Big[[D\psi_0(z)]^2-\psi_0(z)D\psi_0(z)[\alpha(z)+2\tau]$$
$$+\psi_0^2(z)\left(\tau^2+\alpha(z)\tau+\frac{\alpha^2(z)}{4}\right)\Big]\frac{\alpha^2(z)}{\rho(z)}dz, \tag{15}$$

where the boundary values of ψ_2 are:

$$\psi_2(-L)=\left(-\frac{\alpha(-L)}{2}\psi_1(-L)+D\psi_1(-L)\right)\left(L-\frac{1}{\beta}\right)$$
$$-\frac{1}{\beta}D\psi_0(-L)\Big[-\alpha(-L)L+\frac{\alpha(-L)\beta L^2}{2}$$
$$-e^{\beta L}\left(\frac{3\alpha(-L)}{4\beta}-\frac{\alpha(-L)L}{2}+\frac{\lambda_1}{2\lambda_0}\right)\Big], \tag{16}$$

$$\psi_2(L)=\left(\frac{\alpha(L)}{2}\psi_1(-L)-D\psi_1(-L)\right)\left(L+\frac{1}{\delta}\right)+\frac{1}{\delta}D\psi_0(L)$$
$$\times\Big[-\alpha(L)L-\frac{\alpha(L)\delta L^2}{2}-e^{-\delta L}$$
$$\times\left(\frac{3\alpha(L)}{4\beta}+\frac{\alpha(L)L}{2}-\frac{\lambda_1}{2\lambda_0}\right)\Big]. \tag{17}$$

We do not need to calculate ψ_2 since λ_2 requires only the values of $\psi_2(-L)$ and $\psi_2(L)$, which are given in terms of $\psi_1(-L)$, $\psi_1(L)$, $D\psi_1(-L)$, and $D\psi_1(L)$. The integrals in the λ_2 calculation were solved using the ordinary differential equation (ODE) solver LSODA. More details are given in [21].

2. Compound matrix shooting method

The second method solves the full linearized Eq. (1) numerically with an unconventional shooting method, shooting twice from the lower boundary simultaneously. We write equation (1) as a system of four first-degree equations $D\Phi=\mathbf{A}\Phi$, where $\Phi=(w,Dw,D^2w,D^3w)^T$. We then take two "shot" solutions $\chi=(\tilde{w},D\tilde{w},D^2\tilde{w},D^3\tilde{w})^T$ and $\zeta=(\hat{w},D\hat{w},D^2\hat{w},D^3\hat{w})^T$ with the lower boundary conditions $\chi(-L)=(0,0,1,0)^T$ and $\zeta(-L)=(0,0,0,1)^T$, evaluate at the upper boundary, and form the Wronskian

$$\mathbf{W}(\lambda)=\tilde{w}(L)D\hat{w}(L)-\hat{w}(L)D\tilde{w}(L). \tag{18}$$

A complex number λ is an eigenvalue exactly when $\mathbf{W}(\lambda)=0$.

We are able to avoid a problem of numerical dependence by computing with only the wedge product of the two shots in the numerical code. This method, which we call the compound matrix shooting (CMS) method was described by Ng and Reid [22] as a method to reduce a fourth-order ODE problem to a single initial value problem (which is a boundary value problem in our case). It was then shown by Gersting [23] to greatly increase the speed of computation.

We used the λ calculated from the asymptotic method as a seed value and computed $\mathbf{W}(\lambda)$ for λ varying along a contour about the seed. The winding number of the image about zero counts the number of zeros of $\mathbf{W}$ inside the contour. If the winding number is one, indicating that there is a single eigenvalue inside the contour, then we calculate λ approximately using a formula from de Bruijn [24]:

$$\lambda=\frac{1}{2\pi i}\int_{\Gamma}\frac{D\mathbf{W}(z)}{\mathbf{W}(z)}z dz. \tag{19}$$

Next we use the secant method to converge to a λ that satisfies $\mathbf{W}(\lambda)=0$. In our computations using a fluid cell size matching the experimental cell [3] and the physical parameters of near-critical xenon, the matrix $\mathbf{A}$ was very stiff and required additional scaling [21].

B. Numerical results

For the numerical calculations, we impose horizontal periodic boundary conditions corresponding to the dimensions of the fluid container size used by Berg *et al.* for their numerical and physical experiments on near-critical xenon. Thus we look for solutions with period a in the x direction and b in the y direction and take $a=7.6$ mm, $b=38$ mm, $L=9.50$ mm. The horizontal wave numbers must have the form $k_x=m_x\pi/a$ and $k_y=m_y\pi/b$ where m_x, m_y are integers.

We use the restricted cubic (RC) and van der Waals (vdW) equations of state (as in [4]) for xenon to provide two different descriptions for the near-critical density stratification. Xenon has critical temperature $T_c=289.720$ K and critical density $\rho_c=1110.0$ kg/m^3. We assign the constant shear viscosity a typical value from the viscosity model of

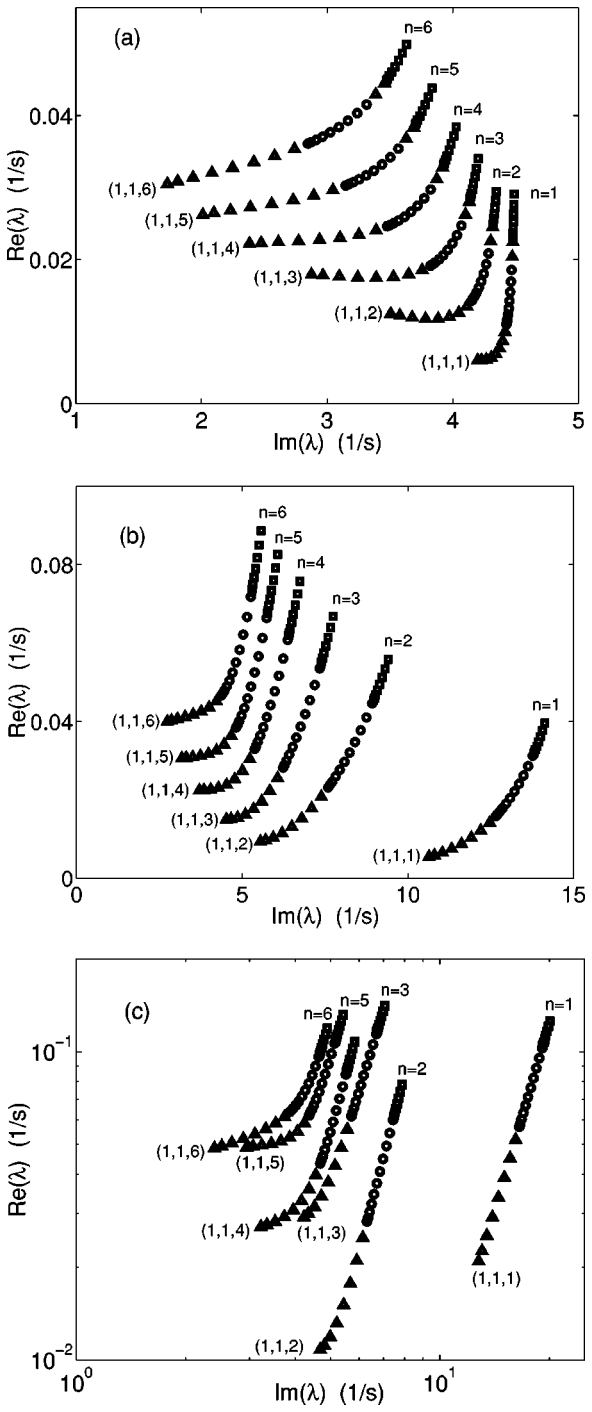

FIG. 2. Comparison of the decay rates vs oscillation frequency at (a) $T=T_c+100$ mK, (b) $T=T_c+10$ mK, and (c) $T=T_c+1$ mK for modes starting at $(1,1,n)$ where $n=1,2,\ldots,6$ using the RC density profile and CMS method with constant viscosity. The $m_x=1$ modes are represented by triangles, the $m_x=2$ modes by circles, and the $m_x=3$ modes by squares. Within each m_x mode family the parameter m_y increases as $\mathrm{Im}(\lambda)$ increases.

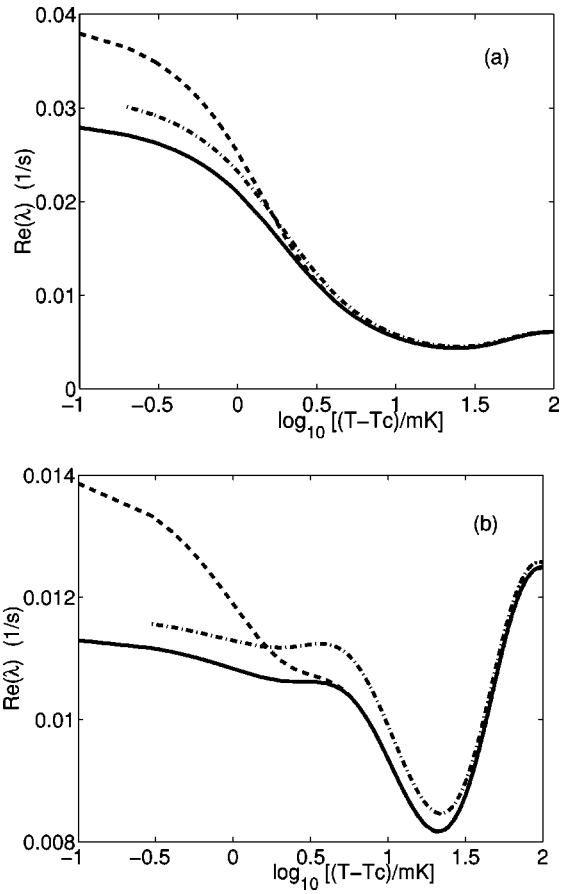

FIG. 3. Comparison of calculated decay rates vs temperature for the RC density profile (a) (1,1,1) and (b) (1,1,2) modes. The dashed line represents the asymptotic method calculation with constant viscosity. The solid line represents the CMS method calculation with constant viscosity. The dash-dotted line represents the CMS method with variable viscosity.

[11] at zero frequency, $\mu=3.2\times10^{-5}$ kg m/s.

Our asymptotic analysis indicates that, in the small-viscosity limit, each eigenvalue λ corresponds to a triplet of integers (m_x,m_y,n). Figure 2 shows the decay rates versus the oscillation frequency at two fixed temperatures for the modes $1\leqslant m_x\leqslant 3$, $1\leqslant m_y\leqslant 11$, and $1\leqslant n\leqslant 6$ for the restricted cubic model density profile computed with the CMS method with constant viscosity. As shown in Fig. 2 each n determines a curve of eigenvalues parametrized by $k=\sqrt{k_x^2+k_y^2}$.

In the interests of brevity, we present further numerical results for the (1,1,1) and (1,1,2) modes only since the damped oscillatory modes with nonzero horizontal wave number described in Theorem 2 exhibit different behavior whether n is odd or even. Figure 2 shows that the $n=1,2$ modes are the slowest decaying modes for the damped oscillatory modes with $m_x=1$ and $m_y=1$. At temperatures far above T_c the $n=1$ is the slowest decaying mode, while very near T_c the $n=2$ mode becomes the slowest decaying mode. This same behavior is shown for the $n=3,4$ and $n=5,6$ modes in Fig. 2.

Figure 3 shows the decay rates $\mathrm{Re}(\lambda)$ in s^{-1} for the (1,1,1) and (1,1,2) modes, plotted versus temperature above critical, for the restricted cubic model density profile, computed with the three-term asymptotic method, the CMS method with constant viscosity, and the CMS method with variable viscosity determined from the model of [11]. Figure 4 shows the same for the van der Waals–derived density profile. The three-term asymptotic expansion provides a good approximation at higher temperatures when the density

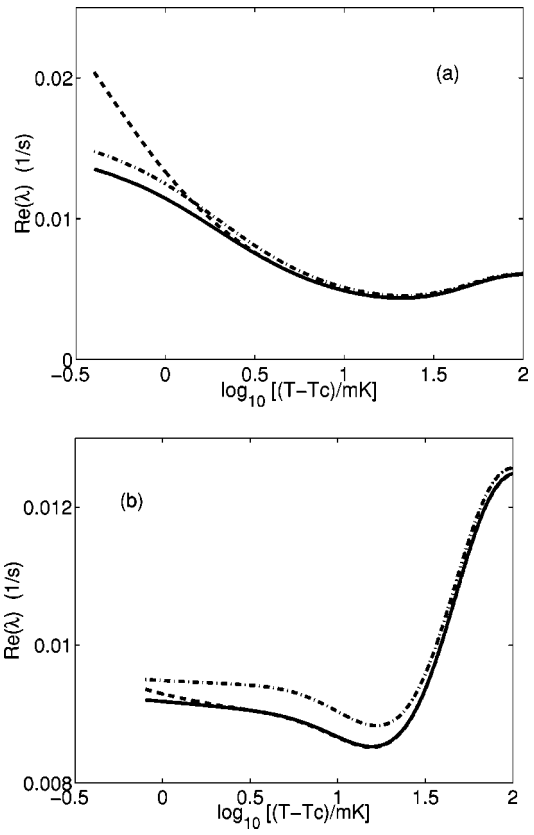

FIG. 4. Comparison of calculated decay rates vs temperature for the vdW-derived density profile (a) (1,1,1) and (b) (1,1,2) modes. The dashed line represents the asymptotic method calculation with constant viscosity. The solid line represents the CMS method calculation with constant viscosity. The dash-dotted line represents the CMS method with variable viscosity.

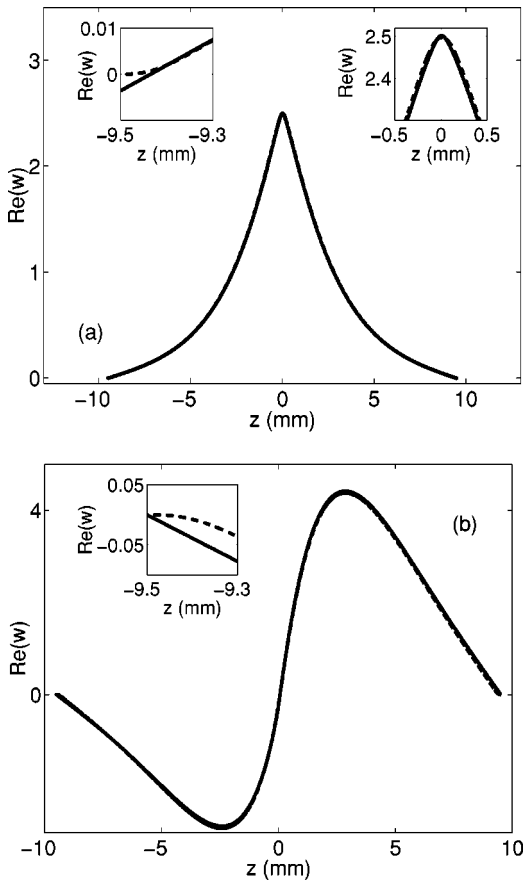

FIG. 5. Comparison of the real part of the eigenfunction for the RC density profile (a) (1,1,1) and (b) (1,1,2) modes.

profile is less steep (at much less computational cost than the other methods), but deviates substantially very close to the critical temperature.

We see that the damping rate grows substantially as the temperature approaches the critical temperature. For the (1,1,1) mode, this increase is approximately 600% for the restricted cubic density profile with the variable-viscosity model as the temperature drops from T_c+20 mK to $T_c+0.3$ mK. This corresponds to a decrease in the decay time λ^{-1} from 219 s at T_c+20 mK to 34 s at $T_c+0.3$ mK. The damping rate for the (1,1,2) mode experiences a significant drop around $T=T_c+20$ mK, but returns to approximately the same value as at $T=T_c+100$ mK.

In Figs. 5 and 6 we compare the real part of the eigenfunction $w(z)$ calculated from the asymptotic method with the real part of the eigenfunction calculated from the CMS method with constant viscosity. We normalized these eigenfunctions so that

$$\int_{-L}^{L}\alpha(z)|w_{\mathrm{CMS}}(z)|^2dz=\int_{-L}^{L}\alpha(z)|w_{\mathrm{Asy}}(z)|^2dz. \quad (20)$$

This normalization determines w_{CMS} and w_{Asy} uniquely within a complex phase factor, which was then estimated.

We plot results for the (1,1,1) and (1,1,2) modes for the restricted cubic method profile and the van der Waals–derived density profile at $T=T_c+1$mK. For the (1,1,1) mode a corner forms in the wave function as $T\rightarrow T_c$. Because of the representation of the horizontal velocity in Eq. (2) in terms of Dw, this indicates that a strong shearing layer develops near the incipient singularity in the density gradient. This provides a mechanism to explain the dramatic enhancement in the decay rate for the (1,1,1) modes as $T\rightarrow T_c$. Unlike the (1,1,1) mode, we see that the wave function for the (1,1,2) mode does not develop a corner. So we see a smaller increase in the decay rate as $T\rightarrow T_c$ for this mode.

C. Mechanism of enhanced damping

Wave damping in slightly viscous fluids is frequently dominated by boundary layer effects. To study this issue for internal waves in a critical fluid, we write $\lambda=\lambda_R+i\lambda_I$ and obtain an integral expression for the damping rate λ_R from the energy dissipation identity. From this expression the main sources of dissipation can be identified.

From the linearized Navier-Stokes equation with constant viscosity and linearized continuity equation, for a single-mode solution the dissipation of the kinetic energy of the system is given by

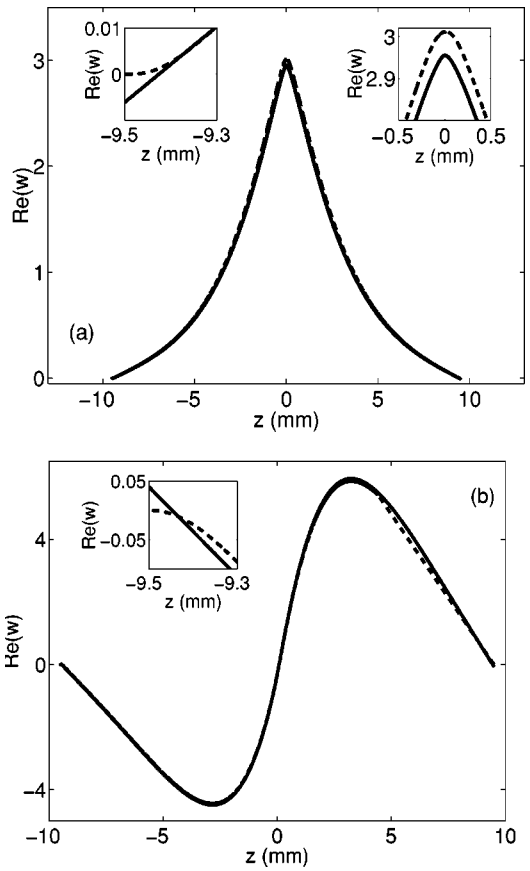

FIG. 6. Comparison of the real part of the eigenfunction vs. height for the vdW-derived density profile (a) (1,1,1) and (b) (1,1,2) modes.

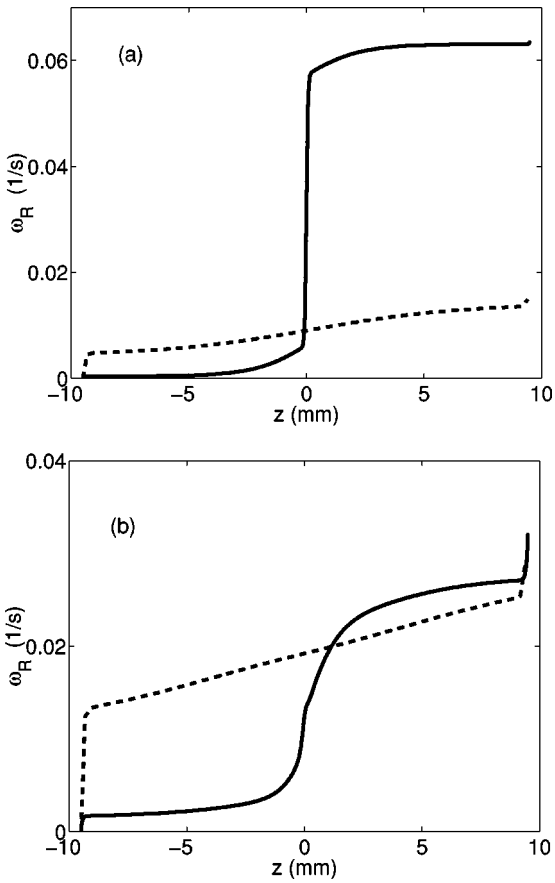

FIG. 7. Partially integrated dissipation rate as a function of height for RC density profile (a) (1,1,1) and (b) (1,1,2) modes. The solid line represents the dissipation rate at $T=T_c+1$ mK and the dashed line at $T=T_c+100$ mK.

$$\frac{d}{dt}(E_k) = -2\lambda_R(E_k)$$

$$= -\lambda_R e^{-2\lambda_R t}\int \rho|\mathbf{u}(\mathbf{r})|^2 d\mathbf{r}$$

$$= e^{-2\lambda_R t}\int \left(-\mu\left|\nabla\mathbf{u}(\mathbf{r})\right|^2 - \frac{\lambda_R}{|\lambda|^2}\left|w(z)\right|^2 gD\rho\right) d\mathbf{r}. \tag{21}$$

Therefore we can write λ_R as

$$\lambda_R = \frac{\int \mu|\nabla\mathbf{u}(\mathbf{r})|^2 d\mathbf{r}}{\int \rho|\mathbf{u}(\mathbf{r})|^2 d\mathbf{r} - \int |\lambda|^{-2}|w(z)|^2 gD\rho d\mathbf{r}}. \tag{22}$$

In order to illustrate the main contributions to the damping rate from the boundary layer and the fluid volume, we perform a partial integration of the numerator in Eq. (22) from the bottom $z=-L$ to an arbitrary level $z=\hat{z}$, and refer to the resulting function of $\hat{z}$ as $\lambda_R(\hat{z})$.

In Fig. 7 we plot $\lambda_R(\hat{z})$ vs $\hat{z}$ for the restricted cubic density profile (1,1,1) and (1,1,2) modes. The results plotted for temperature T_c+100 mK indicate that far above the critical temperature the dissipation rate is substantially influenced by both boundary layer and volumetric effects for both modes. Near the critical temperature (within 1 mK) the dissipation rate for the (1,1,1) mode is dominated by contributions from the shearing layer close to the center. The (1,1,2) mode shows less dominance by volumetric effects over boundary layer effects near the critical temperature. This is consistent with the evidence from Fig. 5 that in this case no strong shearing layer develops close to the center.

V. CONCLUSIONS

Any stably stratified fluid modeled by the incompressible, constant-viscosity Navier-Stokes equations with a sufficiently smooth density profile will admit nonoscillatory linear modes with arbitrarily small damping rates in a periodically confined fluid layer. These modes correspond physically to strongly overdamped slow oscillations of thin fluid layers between consecutive points where vertical velocity vanishes.

The damping of oscillatory internal-wave modes in near-critical xenon is substantially influenced by both boundary layer and volumetric effects at temperatures well above the critical temperature. Horizontal shearing layers at the top and bottom create the boundary layer dissipation. As the temperature of the fluid approaches the critical temperature, the density stratification steepens on the approach to the two-phase regime. During this transition an additional shearing layer can form at the incipient interface between liquid and

vapor, leading to a large magnification in the damping rate. This occurs for modes having eigenfunctions that peak where the density gradient is maximized. Internal-wave modes having eigenfunctions without peaks do not develop a strong central shearing layer. Consequently these wave modes do not exhibit a large increase in the damping rate as the temperature approaches critical. Since in this study we have used periodic boundary conditions in the horizontal directions, we cannot make any statements about any potential effects of side boundaries.

ACKNOWLEDGMENTS

This work was partially supported by the National Science Foundation under Grant No. DMS-97-04924 and SCREMS Grant No. DMS-96-28467.

[1] R. G. Rehm, J. Res. Natl. Bur. Stand., Sect. B **80B**, 353 (1976).
[2] J. Lighthill, *Waves in Fluids* (Cambridge University Press, Cambridge, 1978).
[3] R. F. Berg, M. J. Lyell, G. B. McFadden, and R. G. Rehm, Phys. Fluids **8**, 1464 (1996).
[4] D. M. Anderson and G. B. McFadden, Phys. Fluids **9**, 1870 (1997).
[5] H. Boukari (private communication).
[6] R. W. Gammon, J. N. Shaumeyer, M. E. Briggs, H. Boukari, and D. Gent, in *Light Scattering and Photon Correlation Spectroscopy*, Vol. 40 of *NATO Advanced Study Institute, Series B: Physics*, edited by E. R. Pike and J. B. Abbis (Kluwer Academic, Dordrecht, 1997).
[7] H. Boukari, D. A. Gent, M. E. Briggs, J. N. Shaumeyer, and R. W. Gammon, Phys. Rev. E (to be published).
[8] N. K. Askerov, S. G. Krein, and G. I. Laptev, Funct. Anal. Appl. **2**, 115 (1968).
[9] C. Martel and E. Knobloch, Phys. Rev. E **56**, 5544 (1997).
[10] S. A. Gabov and G. Yu. Malyshev, USSR Comput. Math. Math. Phys. **24**, 170 (1984).
[11] R. F. Berg, M. R. Moldover, and G. A. Zimmerli, Phys. Rev. Lett. **82**, 920 (1999).
[12] M. R. Moldover, J. V. Sengers, R. W. Gammon, and R. J. Hocken, Rev. Mod. Phys. **51**, 79 (1979).
[13] D. Denny and R. L. Pego, Q. Appl. Math. **58**, 103 (2000).
[14] J. G. Liu (private communication).
[15] J. T. Ho and J. D. Listner, Phys. Rev. B **2**, 4523 (1970).
[16] I. Gohberg, S. Goldberg, and M. A. Kaashoek, *Classes of Linear Operators* (Birkhäuser Verlag, Boston, 1990), Vol. I.
[17] K. F. Gurski and R. L. Pego (unpublished).
[18] A. H. Nayfeh, *Introduction to Perturbation Techniques* (Wiley-Interscience, New York, 1981).
[19] P. B. Bailey, B. S. Garbow, H. G. Kaper, and A. Zettl, ACM Trans. Math. Softw. **17**, 500 (1991); http://www.netlib.org/toms/700.
[20] M. R. Scott and H. A. Watts, SIAM (Soc. Ind. Appl. Math.) J. Numer. Anal. **14**, 40 (1977); http://www.netlib.org/slatec/src/dbvsup.f.
[21] K. F. Gurski, Ph.D. thesis, University of Maryland, College Park, 1999.
[22] B. S. Ng and W. H. Reid, J. Comput. Phys. **30**, 125 (1979).
[23] J. M. Gersting, Jr., Comput. Math. Appl. **6**, 167 (1980).
[24] N. G. de Bruijn, *Asymptotic Methods in Analysis* (North-Holland, Amsterdam, 1961).